Published in final edited form as:

Neurobiol Aging. 2018 October ; 70: 265–275. doi:10.1016/j.neurobiolaging.2018.07.006.

Modeling white matter tract integrity in aging with diffusional kurtosis imaging

Andreana Benitez[a,b,c,*], **Jens H. Jensen**[a,c,d], **Maria Fatima Falangola**[a,c,d], **Paul J. Nietert**[e], and **Joseph A. Helpern**[a,b,c,d]

[a]Center for Biomedical Imaging, Medical University of South Carolina, Charleston, SC, USA

[b]Department of Neurology, Medical University of South Carolina, Charleston, SC, USA

[c]Department of Radiology and Radiological Science, Medical University of South Carolina, Charleston, SC, USA

[d]Department of Neuroscience, Medical University of South Carolina, Charleston, SC, USA

[e]Department of Public Health Sciences, Medical University of South Carolina, Charleston, SC, USA

Abstract

Myelin breakdown and neural fiber loss occur in aging. This study used white matter tract integrity metrics derived from biophysical modeling using Diffusional Kurtosis Imaging to assess loss of myelin (i.e., extraaxonal diffusivity, radial direction, $D_{e,\perp}$) and axonal density (i.e., axonal water fraction) in cognitively unimpaired older adults. Tract-based spatial statistics and region of interest analyses sought to identify ontogenic differences and age-related changes in white matter tracts using cross-sectional and longitudinal data analyzed with general linear and mixed-effects models. In addition to pure diffusion parameters (i.e., fractional anisotropy, mean diffusivity, mean kurtosis), we found that white matter tract integrity metrics significantly differentiated early- from late-myelinating tracts, correlated with age in spatially distinct regions, and identified primarily extraaxonal changes over time. Percent metric changes were |0.3-0.9|% and |0.0-1.9|% per year using cross-sectional data and longitudinal data, respectively. There was accelerated decline in some late- versus early-myelinating tracts in older age. These results demonstrate that these metrics may inform further study of the transition from age-related changes to neurodegenerative decline.

Keywords

Aging; White matter; White matter tract integrity Diffusion MRI; Diffusional kurtosis imaging

[*]Corresponding author at: Center for Biomedical Imaging, Medical University of South Carolina, 96 Jonathan Lucas Street, MSC 606, Charleston, SC 29425, USA. Tel.: þ1 843 876 2479. benitez@musc.edu (A. Benitez).

Disclosure statement

The authors have no conflicts of interest to disclose.

1 Introduction

Structural changes in the aging human brain have been well- documented using magnetic resonance imaging (MRI). In addition to gray matter loss most consistently found in frontal and temporal regions (Fjell et al., 2009; Raz and Rodrigue, 2006; Salat, 2004), numerous studies have identified significant and widespread white-matter degeneration with advanced age (Lockhart and DeCarli, 2014). Postmortem histopathological research identifies multiple mechanisms by which this occurs, including loss of myelin in cortico-cortical fibers, insufficient remyelination, reduced length of myelinated fibers, impaired oligodendrocyte regeneration and repair, greater immunoreactivity, and glial senescence (Bartzokis, 2004; Conde and Streit, 2006; Kemper, 1994). As optimum cogni- tive functioning is predicated on efficient and synchronous white matter connections (Bennett and Madden, 2014), it is believed that white matter degeneration accounts for age-related cognitive decline. Consequently, developing tools that measure specific white matter changes is critical for studying cognitive aging and neuro- degenerative diseases for which age is the greatest risk factor.

1.1 Diffusion tensor imaging of aging

Most MRI studies of white matter changes associated with brain aging have used diffusion tensor imaging (DTI). Like all diffusion MRI techniques, DTI is sensitive to the micron-scale displacement of water and can be used to characterize microstructural properties of tissue (Basser and Pierpaoli, 1996). The most commonly reported DTI scalar metrics are fractional anisotropy (FA) and mean diffu-sivity (MD). FA is an index of the directional variability of water diffusion and is scaled from 0 to 1, where values closer to 1 imply greater directional coherence, such as in white matter fiber bundles. On the other hand, MD is an average of the magnitudes of diffusion in 3 orthogonal directions, where higher values imply fewer barriers to diffusion (as in cerebrospinal fluid, where MD is highest). In studies of aging, it has been uniformly reported that FA decreases and MD increases with age; these changes are usually attributed to myelin loss and are often found in superior/anterior regions or present with an anterior-posterior gradient (Madden et al., 2009, 2012; Sullivan and Pfefferbaum, 2006). Such consensus in find- ings have led many to postulate that white matter degenerates in a manner that recapitulates neurodevelopment but in reverse, whereby regions that myelinate last are first to degenerate. This effect, referred to as “retrogenesis” or the “myelodegeneration hy- pothesis,” underscores the age-dependence of neurodegenerative diseases, in which pathology is observed to first arise in late- myelinating regions (Bartzokis, 2011; Braak and Braak, 1996; Davis et al., 2009; Reisberg et al., 1999).

1.2 Diffusional kurtosis imaging of aging

Since its introduction in the 1990s, it has long been appreciated that DTI is limited in its ability to characterize tissue microstructure (Le Bihan and Johansen-Berg, 2012). Diffusional kurtosis imaging (DKI) is one clinically feasible diffusion MRI approach that enhances the fidelity with which tissue microstructure can be characterized. To accomplish this, the monoexponential signal model of DTI is modified by including in the exponent a term quadratic in the b- value (Jensen and Helpern, 2010). In contrast to DTI which assumes a Gaussian distribution of water displacement (i.e., diffusion), DKI adds this higher order

term to account for non-Gaussian diffusion effects. Non-Gaussian diffusion results from barriers to diffusion (e.g., cell membranes, organelles) and water compartmentalization (e.g., extracellular and intracellular), which are inherent to all bio- logical tissues (Jensen and Helpern, 2010). Mean kurtosis (MK) is the principal metric that indexes the complexity of tissue micro- structure (i.e., distribution of structures with subvoxel length scales [typically 1 to 30 microns] including membranes, myelin sheaths, and so forth). Thus, MK decreases in late life as does tissue micro- structural complexity due to a variety of potential causes including myelin breakdown, increased membrane permeability, axonal loss, or edema (Coutu et al., 2014; Das et al., 2017; Falangola et al., 2008; Gong et al., 2014).

1.3 Microstructure modeling of white matter: white matter tract integrity metrics

Empirical diffusion measures, whether derived from DTI or DKI, are nonetheless limited in specificity as they can be affected by different features of tissue microstructure. Thus, a recent trend in the field of diffusion MRI is to develop descriptive models that relate tissue parameters directly to the signal (Panagiotaki et al., 2012). Our group proposed a biophysical model that relates DKI parameters directly to white matter microstructure (Fieremans et al., 2011). This model applies to highly aligned fiber bundles and partitions water into 2 compartments, the intra- and the ex- tra-axonal space. We focus on 2 of these white matter tract integrity (WMTI) metrics: axonal water fraction (AWF) and extra- axonal radial diffusivity ($D_{e,\perp}$). The basic assumptions for the calculation of AWF are that axons are idealized as coplanar, thin cylinders, and that water exchange between the axons and the extra-axonal environment can be neglected. $D_{e,\perp}$ is the diffusivity of the extra-axonal compartment in the radial direction. Both AWF and $D_{e,\perp}$ have compelling support from validation studies using cuprizone-induced demyelination and hypomyelination knockout models (Falangola et al., 2014; Guglielmetti et al., 2016; Jensen et al., 2017; Kelm et al., 2016). Noteworthy is the finding of a double dissociation: in the corpus callosum of cuprizone-fed mice, AWF correlates with tissue AWF (measured by electron micro- scopy) but not with the g-ratio (a marker of demyelination), whereas $D_{e,\perp}$ correlates with the g-ratio but not with tissue AWF (Jelescu et al., 2016).

Although WMTI metrics should not be regarded as having high accuracy, they may serve as indices that help interpret the bio- physical significance of changes in the pure diffusion parameters determined by DKI. For instance, WMTI metrics have been shown to provide disease-relevant information over and above diffusion measures in a number of clinical studies. WMTI metrics correlate with axonal injury in mild traumatic brain injury (Grossman et al., 2015), detect subconcussive head impacts (Davenport et al., 2016), differentiate multiple sclerosis patients from controls (de Kouchkovsky et al., 2016), characterize intraaxonal changes in ischemic white matter lesions (Hui et al., 2012), and distinguish different stages of Alzheimer's disease where late-myelinating tracts show greater degeneration than early-myelinating tracts (Benitez et al., 2014; Fieremans et al., 2013). In characterizing early brain development, AWF and $D_{e,\perp}$ were found to non-linearly in- crease and decrease (respectively) in a manner consistent with well-established observations of asynchronous myelination and pruning from primary sensorimotor, early-myelinating areas to the late-myelinating areas that facilitate higher order cognitive functions (Jelescu et al., 2015). No published studies have tested

whether these metrics can characterize the extent to which aging inversely recapitulates this neurodevelopmental process.

1.4 Study purpose

Thus, we sought to demonstrate that WMTI metrics reflect age- related changes in white matter with topographical differences that correspond with white matter ontogeny. These results were pre- sented alongside standard diffusivity (FA, MD) and kurtosis (MK) metrics. Fig. 1 depicts these parametric maps for 60-, 70-, and 80- year-old participants. Standard and widely-implemented voxel- wise and atlas-based region-of-interest (ROI) image analyses were used to facilitate future replication of these findings. We hypothe- sized that (1) WMTI metrics would differentiate early-myelinating (i.e., splenium of the corpus callosum and projection tracts) from late-myelinating (i.e., body and genu of the corpus callosum, asso- ciation, and limbic) tracts and (2) WMTI metrics in widespread voxels would significantly correlate with age (using cross-sectional data) and detect annual change (using longitudinal data). We expect that rates of change would exceed those reported in longi- tudinal studies of aging cortical and gray matter (i.e., ~0.5%-1.0% of tissue volume loss per year (Fjell et al., 2009, 2014)), particularly in late-myelinating tracts given that loss of synapses, nerve fibers, and myelin typifies the structural changes that underlie cognitive decline in aging nonhuman primates (Peters and Kemper, 2012).

2 Methods

2.1 Participants and procedures

Participants ages 60 to 80 were recruited from the community using on- and off-campus advertisements and mailers to undergo brain MRI, fasting blood draw, neuropsychological testing, and self-report inventories. Eligibility criteria included having English as a first language, no prior diagnosis of a significant neurologic disease (e.g., stroke, epilepsy, dementia) or serious mental illness (e.g., schizophrenia, bipolar disorder), or other poorly controlled or intractable disease with known systematic effects on cognitive function (e.g., untreated diabetes, heart or thyroid disease, can- cer), no contraindications for MRI scanning and a fasting blood draw, sufficient visual and hearing acuity to undergo testing, a score of 23 or greater on the Montreal Cognitive Assessment (MoCA) per suggested cutoff for community-dwelling older adults (Luis et al., 2009) and intact performance on the neuropsycho- logical test battery of the Alzheimer's Disease Centers' uniform data set (Shirk et al., 2011; Weintraub et al., 2009).

Sixty-five participants were enrolled from October 2013 to April 2015, and all were consented under a protocol approved by the Medical University of South Carolina Institutional Review Board. Of these participants, 11 were excluded due to claustrophobia or MRI safety concerns (n = 4), incidental findings deemed clinically sig- nificant by a neuroradiologist (n = 3), below cutoff scores on the MoCA (n = 3), and abnormal neuropsychological test results despite having a MoCA score above the cutoff (n = 1). Of the remaining 54 participants, 72% (n = 39) returned for follow-up after 15.2 ± 3.2 months. Table 1 provides the relevant demographic and medical history variables for the cross-

sectional (i.e., those who completed baseline visits) and longitudinal (i.e., those who completed baseline and follow-up visits) samples.

2.2 MRI acquisition

MRI experiments were conducted on a 3T TIM Trio MR system (Siemens Medical Solutions, Erlangen, Germany) with the following protocol: (1) 3D T1-weighted imaging using an MPRAGE sequence with these parameters: TR/TI/TE = 1900/900/2.26 ms, FOV = 256 × 256 mm2, a generalized autocalibrating partially parallel acquisition (GRAPPA) factor of 2, 1 × 1 × 1 mm3 voxels (scan duration: 4 minutes, 26 seconds). (2) T2-FLAIR sequence with these parameters: TR/TI/TE = 9000/2500/79.0 ms, FOV = 220 × 220 mm2,a GRAPPA factor of 2, voxel size 0.9 × 0.9 × 3 mm3 (scan duration: 4 minutes, 14 seconds). (3) DKI was acquired using single-shot, twice-refocused echo planar imaging to reduce eddy current distortion (Reese et al., 2003), with these parameters: 3 b-values (0, 1000, 2000 s/mm2) along 64 diffusion-encoding directions, voxel size 2.5 × 2.5 × 2.5 mm3, 1 average, TR/TE = 8300/103 ms, FOV = 220 × 220 mm2, a GRAPPA factor of 2, using a proprietary, vendor- supplied gradient table (scan duration: 18 minutes, 17 seconds). There were a total of 25 separate acquisitions with b-value set to zero and identical image parameters (scan duration: 3 minutes, 46 seconds) to minimize the effect of signal noise on parameter estimates (Jones et al., 1999).

2.3 Image processing and analysis

Raw diffusion images were first visually inspected for image quality by a trained image analyst. All DKI acquisitions were denoised with a principal components analysis technique (Veraart et al., 2016b) and Gibbs ringing artifact reduction (Kellner et al., 2016; Veraart et al., 2016a) prior to additional processing utilizing in-house software (diffusional kurtosis estimator (Tabesh et al., 2011)), for registration and estimation of the diffusion and kurto- sis tensors. Five of 54 baseline and 4 of 39 follow-up DKI acquisi- tions had 1e3 volumes with signal dropouts due to motion, and therefore, these volume directions were excluded from the calcu- lation of parametric maps. With 64 diffusion encoding directions, such omissions do not substantially influence the quality of the parametric maps. Calculations of the WMTI metrics (i.e., AWF, $D_{e,\perp}$) followed previously described methods (Fieremans et al., 2011), which added negligible processing time. Non-brain tissue was removed using the Brain Extraction Tool from FSL (FMRIB Software Library, Oxford, UK, http://www.fmrib.ox.ac.uk/fsl/). A fractional intensity threshold of 0.3 resulted in optimum nonbrain tissue extraction, verified via visual inspection.

Two standard analysis techniques were used: voxelwise anal- ysis using tract-based spatial statistics (TBSS; Smith et al., 2006) and ROI analysis. In TBSS, all subject FA images were non-linearly registered into standard FMRIB58_FA space, and a mean FA image was generated and thresholded to create the mean FA skeleton. All other subject parametric maps were then projected onto this FA skeleton and thresholded accordingly (i.e., FA = 0.2 for diffusivity and kurtosis metrics and FA = 0.4 for WMTI metrics since the model is valid only for highly aligned fibers) for further statistical analysis on the skeletonized voxels. Results were binarized and visualized using BrainNet Viewer (Xia et al., 2013). The TBSS-processed, non-skeletonized maps were then subjected to ROI analyses, extracting the mean

metric values for each ROI using the Johns Hopkins ICBM-DTI-81 atlas (Mori et al., 2005). We opted not to exclude the voxels with increased T2-signal in white matter for conceptual and pragmatic reasons described in Supplementary Material A.

2.4 Statistical analyses

Statistical analysis of ROIs was performed using IBM SPSS, version 24. The corpus callosum ROIs (i.e., genu, body, splenium) were obtained as is through the atlas (see Fig. 2). We then prepared the other ROIs by creating 3 composite variables. We selected 3 tracts per tract type: projection tracts (corticospinal tract, cerebral peduncles, and posterior limb of the internal capsule), association tracts (superior longitudinal fasciculus, superior fronto-occipital fasciculus, and sagittal stratum) and limbic tracts (cres of the fornix, uncinate fasciculus, and cingulum [hippocampus]). We averaged the bilateral ROIs, and then averaged the 3 ROIs per tract type to create the composites reported here (see Supplemental Table 1 for the metric values of each ROI). We then examined all variables to ensure that they met the necessary statistical assumptions.

We ran within-subjects general linear models to assess tract differences in baseline metrics for the cross-sectional data and in annualized percent metric change from baseline (i.e., [(follow-up metric - baseline metric)/follow-up period in years]/baseline metric) for the longitudinal data. We ran linear mixed-effects models with tract type and age as fixed effects and subjects as random effects. Cross-sectional models used baseline raw metric values for each tract and baseline age. Longitudinal models used annualized percent metric change from baseline and the average age between baseline and follow-up. We ran 2 sets of models: 1 for the corpus callosum ROIs (i.e., splenium, body, and genu) and the other for the projection, association, and limbic tracts. Our first hypothesis would be supported if we found significant differences across tract types (i.e., early- vs. late-myelinating tracts). Our sec- ond hypothesis would be supported if we found significant main effects for age and interaction effects whereby late-myelinating tracts would have greater rates of change than early-myelinating tracts.

Voxelwise analysis was performed using FSL's randomise (Winkler et al., 2014). First, we tested whether baseline age was correlated with WMTI metrics. Second, we created difference maps (i.e., follow-up minus baseline skeletonised metric maps) using fslmaths and using 1-sample t tests, and we tested whether these differences were significantly greater than 0, covarying for follow-up time in years and average age between baseline and follow-up. We used 5000 permutations with threshold-free cluster enhancement and a statistical significance level set at $p < 0.05$, corrected for multiple comparisons.

3 Results

3.1 WMTI metrics and white-matter ontogeny

WMTI metric values differed according to white matter ontogeny in the hypothesized directions (Table 2, Fig. 3A). As pre- dicted, AWF was significantly greater in early-myelinating tracts (i.e., splenium, projection tracts) than in late-myelinating tracts (i.e., body, genu, association, and limbic tracts), while $D_{e,\perp}$ was greater in the late-myelinating than in

the early-myelinating tracts. Findings were similarly significant in the expected directions for FA, MD, and MK. Across all metrics, the difference between the body and the genu was no more than moderate (d = |0.0-0.5|) while the largest difference was between the projection and limbic tracts (d = |2.3-7.5|). AWF, FA, and MK differentiated the non-corpus callosum tracts with the greatest effect sizes (d = |2.8-7.5|, d = |1.8-6.8|, and d = |2.6-6.4|, respectively), although all other contrasts except for the body and genu had large effect size differences (i.e., d > |0.8|) as well. In sum, WMTI metrics differentiated early- from late-myelinating tracts in a manner that is consistent with results us- ing pure diffusion parameters, with slightly larger effect sizes in the case of AWF.

3.2 WMTI metrics and aging

WMTI metrics and pure diffusion parameters reflected age- related changes in white matter, with nuances depending on ana- lytic approach (i.e., ROI or voxelwise), and study design (i.e., cross- sectional or longitudinal). Briefly, ROI analyses showed that all regional metrics correlated with age and most changed over time. Results from the cross-sectional and longitudinal analyses differed in terms of which regional metrics were estimated to change at greater rates at older ages (i.e., $D_{e,\perp}$, MD) or over time (i.e., MK). Voxelwise analyses indicated spatially distinct correlations with age across all metrics, but only a subset of these (i.e., $D_{e,\perp}$, FA, MD) significantly changed over time, with spatially similar results.

3.2.1 ROI analysis—ROI analysis results differed according to study design. Using cross-sectional data, mixed-effects models resulted in two main findings (Table 3, Fig. 3B). First, there were significant main effects of tract type and age for AWF, FA, and MK, but no interaction effects. That is, these metrics in the corpus callosum and other tracts, while significantly different from one another, demonstrated similar as- sociations with age. There also was no interaction effect for $D_{e,\perp}$ in the corpus callosum tracts. Using the data from these models to estimate annual change, the changes in all these metrics were |0.3-0.9|% per year. Second, for MD in the corpus callosum and both MD and $D_{e,\perp}$ in the other tracts, there were interactions between tract type and age. That is, these metrics changed with age, but some tracts changed at greater rates. Specifically, with increased age, MD in the late-myelinating genu increased at greater rates (i.e., 0.7%-0.9% per year) than MD in the body or the splenium (i.e., 0.5%-0.7% per year). Similarly, both $D_{e,\perp}$ and MD in the late-myelinating limbic tracts changed at greater rates (i.e., 0.7%-0.8% per year) than both metrics in the early-myelinating projection tracts (0.3%-0.4% per year).

In contrast, analyses using the longitudinal data (Table 4) identified a much broader range of annualized percent changes across all metrics (i.e., |0.0-1.9|% per year), with the greatest rates in the projection, association, and limbic tracts for FA (−1.0-1.9% per year), $D_{e,\perp}$ (1.3%-1.7% per year), and MD (1.1%-1.5% per year). Rates of change in the corpus callosum were consistent with cross- sectional estimates but were higher for FA and $D_{e,\perp}$ in the genu (i.e., 1.2% and 1.0% per year, respectively). None of these annual percent changes were significantly different across tracts except for FA, where annual percent change in FA was significantly greater in projection than in limbic tracts. A few of the annual change estimates (i.e., AWF and MK in the body, MK in the genu, association, and limbic tracts) were in the positive direction (i.e., opposite of what was estimated based on the cross-

sectional an- alyses); however, these had relatively low magnitudes and large standard deviations. Linear mixed-effects models did not identify age by tract type interactions for any of the annualized percent metric changes (data not shown) with the exception of MK in the corpus callosum, $F(74) = 3.3$, $p = 0.04$. That is, annualized percent MK change in the splenium increased with age (b = 0.002, $p = 0.01$) relative to the genu. Apart from this, late-myelinating tracts did not appear to change with age at greater rates than early- myelinating tracts, and tracts were not changing at greater rates at older ages.

3.2.2 Voxelwise analysis—Voxelwise analysis results differed according to study design. Using cross-sectional data, all metrics significantly correlated with age ($p < 0.05$) in the expected directions (i.e., age negatively correlated with AWF/FA/MK and positively correlated with $D_{e,\perp}$/ MD). FA had the most number of voxels (i.e., 51.6%) that signifi-cantly correlated with age followed by AWF (34.5%) and $D_{e,\perp}$ (31.3%), then MK (16.4%) and MD (15.0%, Fig. 3A1). Fig. 4 A2 depicts the spatial distribution of these correlations. Here, AWF negatively correlated with age in bilateral anterior voxels, while $D_{e,\perp}$ posi- tively correlated with age in posterior voxels. FA correlated with age in widespread voxels, whereas MD and MK correlated with age in fewer medial voxels.

Using longitudinal data, voxelwise analyses showed that $D_{e,\perp}$, FA, and MD significantly changed from baseline to follow-up, con- trolling for interval time and age. Changes were in the expected directions (i.e., decreased FA and increased $D_{e,\perp}$, MD), with MD having the most number of voxels (i.e., 49.8%) that significantly changed followed by $D_{e,\perp}$ (41.6%) and FA (35.0%; Fig. 3B1), with a bilateral anterior spatial pattern of correlations (Fig. 4B2). Supplemental Fig. 1 presents these cross-sectional and longitudinal voxelwise results in multiple planes and slices.

4. Discussion

This study sought to demonstrate that WMTI metrics reflect ontogenic differences and age-related changes in white matter. Consistent with our hypotheses, we found that WMTI metrics distinguished late- from early-myelinating tracts and detected age- related changes in white matter, with some metrics (i.e., $D_{e,\perp}$ and MD) demonstrating greater rates of change in late- versus early- myelinating tracts with aging. This study adds to the robust liter- ature on white-matter changes in aging but uniquely provides evidence that these changes may be more specific to the extra- axonal environment such as myelin breakdown.

4.1 WMTI metrics reflect differences in white-matter ontogeny

Consistent with our prior work (Benitez et al., 2014), WMTI metrics differentiate tracts according to known white-matter ontogeny, whereby early-myelinating tracts have greater axonal density (e.g., greater AWF) and myelin integrity (e.g., lower $D_{e,\perp}$) than late-myelinating tracts, with similar findings for FA, MD, and MK. These results replicate findings from other lifespan DKI studies (Coutu et al., 2014; Das et al., 2017; Gong et al., 2014), but this study includes a large sample of older adults, encompasses more white matter ROI, and reports both cross-sectional and longitudinal es- timates of age-related changes. This article provides benchmark values for different tract types which are critical to developing these metrics as biomarkers of disease. Studies on the early detection of

Alzheimer's disease using complementary MRI tech- niques report changes in late-myelinating brain regions in partic- ular (Dean et al., 2017; Stricker et al., 2016). WMTI metrics can therefore serve as sensitive metrics of changes in these vulnerable areas in diseases for which age is the greatest risk factor.

4.2 WMTI metrics detect age-related changes

Across analytic approaches and study designs, these results validate the extent to which WMTI metrics can index age-related changes. More importantly, this study provides unique insights into how, where, and at what rate white matter degenerates with age. That voxelwise correlations between metrics and age were significant for more anterior voxels for AWF, and more posterior voxels for $D_{e,\perp}$ presents an intriguing dissociation; white-matter degeneration in the frontal lobes may involve axonal loss, whereas myelin breakdown may underlie white-matter changes in parieto- temporal regions. These results corroborate prior literature local- izing white matter changes to these regions in aging (Bartzokis, 2011) but suggest the possibility of differing mechanisms by which these changes occur. Such spatial specificity was not described by FA, MD, or MK. Longitudinal results, however, only point to increased extra-axonal diffusivity (along with significant changes in FA and MD), consistent with established findings that aging primarily involves changes in myelin or glia rather than to neurons and their processes. The longitudinal analyses also iden- tified significant changes in the cerebellum. Although these voxels were relatively few and as such may be of uncertain significance, cerebellum white matter also degrades with age and has important cerebral connections to functionally and ontogenically diverse re- gions (Andersen et al., 2003; Schmahmann and Pandya, 1997). Nonetheless, the reasons for the different spatial distribution be- tween the cross-sectional and longitudinal study designs remain unclear and temper these conjectures regarding the spatial speci- ficity of white matter changes.

Consistent with our hypothesis, metrics that are potentially most sensitive to changes in myelin and glia (i.e., $D_{e,\perp}$ and MD) indexed accelerated declines with age in some late-myelinating tracts compared to early-myelinating tracts. However, we did not confirm this finding in the longitudinal analysis, where we instead found that annual percent MK change in the early-myelinating splenium increased with age compared to the late-myelinating genu. These are intriguing preliminary findings that warrant replication. It is also important to note that the observation of preferential degeneration of late-myelinating regions may be specific to intracortical or juxtacortical myelin (Phillips et al., 2016; Vidal-Piñeiro et al., 2016), rather than to the large fiber bundles on which this paper is focused.

In sum, these findings indicate that white matter degenerates in late life to varying extents and locations, with annual rates of decline that exceed reported changes in cortical and gray matter volume. The metrics with the greatest changes indicate the distinct possibility that myelin breakdown is driving these effects, more so in some late-myelinating tracts. This lends support to the hypoth- esis that age-related myelin breakdown may be a predisposing factor in diseases such as Alzheimer's disease (Bartzokis, 2004, 2011), where white-matter degenereration primarily occurs in late- myelinating tracts. It therefore stands to reason that these WMTI and other metrics may serve as sensitive biomarkers of the tran- sition from

normal aging to the earliest stages of neurodegenerative disease, such that incipient disease may be detected by aberrant extra-axonal diffusivities and more precipitous declines over time that exceed normal age-related changes. Our group is currently engaged in studies to verify these assertions using longitudinal clinical studies of mild cognitive impairment and preclinical Alz- heimer's disease, and preclinical rodent models. Subsequent pub- lications will report the extent to which these metrics relate to age- related changes in cognitive functioning.

4.3 Strengths and limitations

This study has many strengths, including the use of an advanced yet clinically applicable diffusion technique, an innovative bio- physical model of white matter, a longitudinal study design, and the use of statistical models that explicitly test biologically informed hypotheses. The results from the pure diffusion parameters demonstrated trajectories that were concordant with previous studies of lifespan changes (i.e., age 18e80þ years), which include samples of older adults aged 60þ years that are comparable in number to the sample size in this study (Coutu et al., 2014; Lebel et al., 2012; Yeatman et al., 2014). In contrast to a lifespan approach, this study focused on a narrow critical age window to identify changes upon which to focus further research on the impact of aging on the earliest stages of neurodegenerative disease. These findings nonetheless bear replication in future studies with larger and more representative samples.

Given the novelty of these metrics, we prioritized using conventional ROIs and analytical techniques for the ease of replication. Most values here are encouragingly within 1 standard deviation of values reported in prior publications using data that were similarly analyzed but acquired from a different scanner (Fieremans et al., 2013). However, the discrepancy in voxelwise results between study designs suggest that more optimized image registration and processing, alternative ROI identification through tractography or other atlases, or improved clinical screening of the study sample may yield more consistency. Future extensions of this work may include measures of functional connectivity or activation to examine whether specific functions (e.g., sensory, motor, cognitive) can be delineated by modeling parameters. However, recent evidence indicates that age-related structural and functional changes are weakly correlated, suggesting these may be parallel processes with different temporal and spatial trajectories (Fjell et al., 2017; Tsang et al., 2017).

Like many similar studies that use novel techniques and expensive technologies, this study is limited by its convenience sampling methodology, resulting in a demographically homogenous, highly educated sample. There were no gender differences in these metrics (data not shown), but it remains possible that these and other demographic factors may moderate these associations. It is also possible that some participants already have incipient neurodegenerative disease that was not detected, although neuropsychological evaluations at both baseline and follow-up confirmed that at least at the time of the study they were cognitively unimpaired. These results are thus more generalizable to older adults who self-identify as and are confirmed to be cogni- tively intact, and who, like most of the general population of older adults, have at least 1 chronic medical condition (Wolff et al., 2002). Variations or fluctuations in the health status of older adults are beyond experimental control

in observational longitudinal studies. As such, conclusions regarding the extent to which this study adds to new knowledge regarding “typical aging” versus “healthy aging” must be tempered by this caveat.

Another limitation of this study is that it does not comprehensively address all potential mechanisms that contribute to white matter changes. Although we chose to focus our analysis on the most validated and frequently reported metrics, to some extent, other metrics not reported here can inform this question. However, subsequent reanalysis using axial and radial diffusivity (2 other DTI- based metrics) showed largely redundant results (see Supplementary Material B). Briefly, the results for axial and radial diffusivity paralleled the results for MD and $D_{e,\perp}$, respectively, in both the cross-sectional and longitudinal ROI analyses. The longitudinal voxelwise results showed a comparably widespread spatial pattern of increases in all DTI-based diffusivity metrics. Although these findings might suggest superior sensitivity of these metrics to detecting change, these may also indicate their lack of specificity to which aspects of the tissue are changing. Given that $D_{e,\perp}$ but not AWF significantly changed over time, it is possible that the increased diffusivities are a function of changes in myelin/glia rather than axonal density loss. Such results exemplify the potential specificity of white-matter modeling to tissue changes over pure diffusion parameters.

Nonetheless, it is important to note that there is considerable shared variance across these parameters, with the highest correlations between $D_{e,\perp}$ and RD, moderate-to-high correlations between AWF and FA, and variable correlations between MK and MD (cf. Supplemental Table 5 and Supplemental Fig. 4). These metrics are inter-related yet are independently meaningful as evi- denced by the findings in this study. To illustrate, MK is physically distinct from all DTI-derived parameters in that it quantifies an independent property of water diffusion. However, for a specific type of biological tissue or process, MK may be correlated with some DTI parameters because a given microstructural feature can affect multiple diffusion properties. However, this sort of relation- ship is not generic and does not imply an intrinsic dependence of MK (or WMTI metrics) on DTI-derived parameters.

Other diffusion-based microstructure modeling methods may also further disentangle the biological specificity of white-matter changes. While such models (e.g., neurite orientation dispersion and density imaging) qualitatively demonstrate similar trends that reflect known white-matter ontogeny and pathology (e.g., Billiet et al., 2015; Slattery et al., 2017), quantitative estimates derived from various models are model-dependent and remain subject to the limitations of model assumptions, wherein accuracy is sacri- ficed for biological interpretability (Jelescu et al., 2015). More comprehensive diffusion data sets with higher b-values may over- come these limitations, but these acquisitions come at the expense of clinical feasibility. Future extensions of this work will most benefit from using shorter acquisitions given clinical constraints in the aging population. Fortunately, newer MRI systems and tech- niques such as simultaneous multislice imaging are becoming more prevalent. These allow for diffusion data to be obtained with accelerations of 2e4 times that of conventional acquisitions (Feinberg and Setsompop, 2013).

5 Conclusion

This study supports the viability of WMTI (i.e., AWF, $D_{e,\perp}$) and pure diffusion metrics (i.e., FA, MD, MK) as clinically applicable biomarkers that provide insight into the specific mechanisms by which white matter changes with age and may predispose individuals to neurodegenerative disease. Further work is needed to replicate these longitudinal findings with other complementary biomarkers of white-matter changes and incipient disease.

Supplementary Material

Refer to Web version on PubMed Central for supplementary material.

Acknowledgements

The authors thank Anne Sorrell, Dana Szeles, Brianna Jones, Deborah Nelson, Danae Montgomery, Clifford Chan, Corinne McGill, and Madison Hyer for their assistance with participant recruitment, research coordination, and data analysis. They also gratefully acknowledge the study participants for generously offering their time and data for this work. This work was approved by the Insti- tutional Review Board of the Medical University of South Carolina (IRB # Pro 000 28302). This work was supported by the National Institutes of Health (NCATS UL1TR000062/KL2 TR000060 and NIA K23 AG044434 to A.B., NIA R01 AG057602 to J.H.J. and M.F.M., NCATS UL1TR000062 to P.J.N., and NIA R01 AG054159 to J.A.H.) and the Litwin Foundation (to J.A.H.).

References

Andersen BB, Gundersen HJG, Pakkenberg B, 2003 Aging of the human cere- bellum: a stereological study. J. Comp. Neurol 466, 356e365.

Bartzokis G, 2011 Alzheimer's disease as homeostatic responses to age-related myelin breakdown. Neurobiol. Aging 32, 1341e1371.

Bartzokis G, 2004 Age-related myelin breakdown: a developmental model of cognitive decline and Alzheimer's disease. Neurobiol. Aging 25, 5e18 author reply 49–62.

Basser PJ, Pierpaoli C, 1996 Microstructural and physiological features of tissues elucidated by quantitative-diffusion-tensor MRI. J. Magn. Reson. B 111, 209e219.

Benitez A, Fieremans E, Jensen JH, Falangola MF, Tabesh A, Ferris SH,Helpern JA, 2014 White matter tract integrity metrics reflect the vulnerability of late-myelinating tracts in Alzheimer's disease. Neuroimage Clin 4, 64e71.

Bennett IJ, Madden DJ, 2014 Disconnected aging: cerebral white matter integrity and age-related differences in cognition. Neuroscience 276, 187e205.

Billiet T, Vandenbulcke M, Mädler B, Peeters R, Dhollander T, Zhang H, Deprez S, Van den Bergh BRH, Sunaert S, Emsell L, 2015 Age-related microstructural differences quantified using myelin water imaging and advanced diffusion MRI. Neurobiol. Aging 36, 2107e2121.

Braak H, Braak E, 1996 Development of Alzheimer-related neurofibrillary changes in the neocortex inversely recapitulates cortical myelogenesis. Acta Neuro- pathol. (Berl) 92, 197e201.

Conde JR, Streit WJ, 2006 Microglia in the aging brain. J. Neuropathol. Exp. Neurol 65, 199e203.

Coutu J-P, Chen JJ, Rosas HD, Salat DH, 2014 Non-Gaussian water diffusion in aging white matter. Neurobiol. Aging 35, 1412e1421.

Das SK, Wang JL, Bing L, Bhetuwal A, Yang HF, 2017 Regional values of diffusional kurtosis estimates in the healthy brain during normal aging. Clin. Neuroradiol 27, 283e298.

Davenport EM, Apkarian K, Whitlow CT, Urban JE, Jensen JH, Szuch E, Espeland MA, Jung Y, Rosenbaum DA, Gioia GA, Powers AK, Stitzel JD, Maldjian JA, 2016 Abnormalities in diffusional kurtosis metrics related to head impact exposure in a season of high school varsity football. J. Neurotrauma 33, 2133e2146.

Davis SW, Dennis NA, Buchler NG, White LE, Madden DJ, Cabeza R, 2009 Assessing the effects of age on long white matter tracts using diffusion tensor tractography. Neuroimage 46, 530e541.

de Kouchkovsky I, Fieremans E, Fleysher L, Herbert J, Grossman RI, Inglese M, 2016 Quantification of normal-appearing white matter tract integrity in multiple sclerosis: a diffusion kurtosis imaging study. J. Neurol 263, 1146e1155.

Dean DC, Hurley SA, Kecskemeti SR, O'Grady JP, Canda C, Davenport-Sis NJ, Carlsson CM, Zetterberg H, Blennow K, Asthana S, Sager MA, Johnson SC, Alexander AL, Bendlin BB, 2017 Association of Amyloid pathology with myelin Alteration in preclinical Alzheimer disease. JAMA Neurol 74, 41e49.

Falangola MF, Guilfoyle DN, Tabesh A, Hui ES, Nie X, Jensen JH, Gerum SV, Hu C, LaFrancois J, Collins HR, Helpern JA, 2014 Histological correlation of diffusional kurtosis and white matter modeling metrics in cuprizone-induced corpus callosum demyelination. NMR Biomed 27, 948e957.

Falangola MF, Jensen JH, Babb JS, Hu C, Castellanos FX, Di Martino A, Ferris SH, Helpern JA, 2008 Age-related non-Gaussian diffusion patterns in the prefrontal brain. J. Magn. Reson. Imaging 28, 1345e1350.

Feinberg DA, Setsompop K, 2013 Ultra-fast MRI of the human brain with simultaneous multi-slice imaging. J. Magn. Reson 229, 90e100.

Fieremans E, Jensen JH, Helpern JA, 2011 White matter characterization with diffusional kurtosis imaging. Neuroimage 58, 177e188.

Fieremans E, Benitez A, Jensen JH, Falangola MF, Tabesh A, Deardorff RL, Spampinato MVS, Babb JS, Novikov DS, Ferris SH, Helpern JA, 2013 Novel white matter tract integrity metrics sensitive to Alzheimer disease pro- gression. AJNR Am. J. Neuroradiol 34, 2105e2112.

Fjell AM, Sneve MH, Grydeland H, Storsve AB, Amlien IK, Yendiki A, Walhovd KB, 2017 Relationship between structural and functional connec- tivity change across the adult lifespan: a longitudinal investigation. Hum. Brain Mapp 38, 561e573.

Fjell AM, Walhovd KB, Fennema-Notestine C, McEvoy LK, Hagler DJ, Holland D, Brewer JB, Dale AM, 2009 One-year brain atrophy evident in healthy aging. J. Neurosci 29, 15223e15231.

Fjell AM, Westlye LT, Grydeland H, Amlien I, Espeseth T, Reinvang I, Raz N, Dale AM, Walhovd KB, 2014 Accelerating cortical thinning: unique to de- mentia or universal in aging? Cereb. Cortex 24, 919e934.

Gong NJ, Wong CS, Chan CC, Leung LM, Chu YC, 2014 Aging in deep gray matter and white matter revealed by diffusional kurtosis imaging. Neurobiol. Aging 35, 2203e2216.

Grossman EJ, Kirov II, Gonen O, Novikov DS, Davitz MS, Lui YW, Grossman RI, Inglese M, Fieremans E, 2015 N-acetyl-aspartate levels correlate with intra-axonal compartment parameters from diffusion MRI. Neuroimage 118, 334e343.

Guglielmetti C, Veraart J, Roelant E, Mai Z, Daans J, Van Audekerke J, Naeyaert M, Vanhoutte G, Delgado y Palacios R, Praet J, Fieremans E, Ponsaerts P, Sijbers J, Van der Linden A, Verhoye M, 2016 Diffusion kurtosis imaging probes cortical alterations and white matter pathology following cuprizone induced demyelination and spontaneous remyelination. Neuroimage 125, 363e377.

Hui ES, Fieremans E, Jensen JH, Tabesh A, Feng W, Bonilha L, Spampinato MV, Adams R, Helpern JA, 2012 Stroke assessment with diffusional kurtosis imaging. Stroke J. Cereb. Circ 43, 2968e2973.

Jelescu IO, Veraart J, Adisetiyo V, Milla SS, Novikov DS, Fieremans E, 2015 One diffusion acquisition and different white matter models: how does microstructure change in human early development based on WMTI and NODDI? Neuroimage 107, 242e256.

Jelescu IO, Zurek M, Winters KV, Veraart J, Rajaratnam A, Kim NS, Babb JS, Shepherd TM, Novikov DS, Kim SG, Fieremans E, 2016 In vivo quantifi- cation of demyelination and recovery using compartment-specific diffusion MRI metrics validated by electron microscopy. Neuroimage 132, 104e114.

Jensen JH, Helpern JA, 2010 MRI quantification of non-Gaussian water diffusion by kurtosis analysis. NMR Biomed 23, 698e710.

Jensen JH, McKinnon ET, Glenn GR, Helpern JA, 2017 Evaluating kurtosis- based diffusion MRI tissue models for white matter with fiber ball imaging. NMR Biomed 30 10.1002/nbm.3689.

Jones DK, Horsfield MA, Simmons A, 1999 Optimal strategies for measuring diffusion in anisotropic systems by magnetic resonance imaging. Magn. Reson. Med 42, 515e525.

Kellner E, Dhital B, Kiselev VG, Reisert M, 2016 Gibbs-ringing artifact removal based on local subvoxel-shifts: Gibbs-Ringing Artifact Removal. Magn. Reson. Med 76, 1574e1581.

Kelm ND, West KL, Carson RP, Gochberg DF, Ess KC, Does MD, 2016 Evaluation of diffusion kurtosis imaging in ex vivo hypomyelinated mouse brains. Neuroimage 124, 612e626.

Kemper TL, 1994 Neuroanatomical and neuropathological changes during aging and dementia. In: Albert ML, Knoefel JE (Eds.), Clinical Neurology of Aging Oxford University Press, New York, pp 3e67.

Le Bihan D, Johansen-Berg H, 2012 Diffusion MRI at 25: exploring brain tissue structure and function. Neuroimage 61, 324e341.

Lebel C, Gee M, Camicioli R, Wieler M, Martin W, Beaulieu C, 2012 Diffusion tensor imaging of white matter tract evolution over the lifespan. Neuroimage 60, 340e352.

Lockhart SN, DeCarli C, 2014 Structural imaging measures of brain aging. Neu- ropsychol. Rev 24, 271e289.

Luis CA, Keegan AP, Mullan M, 2009 Cross validation of the Montreal Cognitive Assessment in community dwelling older adults residing in the Southeastern US. Int. J. Geriatr. Psychiatry 24, 197e201.

Madden DJ, Bennett IJ, Burzynska A, Potter GG, Chen N, Song AW, 2012 Diffusion tensor imaging of cerebral white matter integrity in cognitive aging. Biochim. Biophys. Acta 1822, 386e400.

Madden DJ, Bennett IJ, Song AW, 2009 Cerebral white matter integrity and cognitive aging: contributions from diffusion tensor imaging. Neuropsychol. Rev 19, 415e435.

Mori S, Wakana S, Nagae-Poetscher L, van Zijl P, 2005 MRI Atlas of Human White Matter Elsevier, Amsterdam, The Netherlands.

Panagiotaki E, Schneider T, Siow B, Hall MG, Lythgoe MF, Alexander DC, 2012 Compartment models of the diffusion MR signal in brain white matter: a tax- onomy and comparison. Neuroimage 59, 2241e2254.

Peters A, Kemper T, 2012 A review of the structural alterations in the cerebral hemispheres of the aging rhesus monkey. Neurobiol. Aging 33, 2357e2372.

Phillips OR, Joshi SH, Piras F, Orfei MD, Iorio M, Narr KL, Shattuck DW, Caltagirone C, Spalletta G, Di Paola M, 2016 The superficial white matter in Alzheimer's disease: superficial White Matter in Alzheimer's Disease. Hum. Brain Mapp 37, 1321e1334.

Raz N, Rodrigue KM, 2006 Differential aging of the brain: patterns, cognitive correlates and modifiers. Neurosci. Biobehav. Rev 30, 730e748.

Reese TG, Heid O, Weisskoff RM, Wedeen VJ, 2003 Reduction of eddy-current- induced distortion in diffusion MRI using a twice-refocused spin echo. Magn. Reson. Med 49, 177e182.

Reisberg B, Franssen EH, Hasan SM, Monteiro I, Boksay I, Souren LE, Kenowsky S, Auer SR, Elahi S, Kluger A, 1999 Retrogenesis: clinical, phys- iologic, and pathologic mechanisms in brain aging, Alzheimer's and other dementing processes. Eur. Arch. Psychiatry Clin. Neurosci 249 (Suppl 3), 28e36.

Salat DH, 2004 Thinning of the cerebral cortex in aging. Cereb. Cortex 14, 721e730.

Schmahmann JD, Pandya DN, 1997 The cerebrocerebellar system. Int. Rev. Neurobiol 41, 31e60.

Shirk SD, Mitchell MB, Shaughnessy LW, Sherman JC, Locascio JJ, Weintraub S, Atri A, 2011 A web-based normative calculator for the uniform data set (UDS) neuropsychological test battery. Alzheimers Res. Ther 3, 32. [PubMed: 22078663]

Slattery CF, Zhang J, Paterson RW, Foulkes AJM, Carton A, Macpherson K, Mancini L, Thomas DL, Modat M, Toussaint N, Cash DM, Thornton JS,Henley SMD, Crutch SJ, Alexander DC, Ourselin S, Fox NC, Zhang H, Schott JM, 2017 ApoE influences regional white-matter axonal density loss in Alzheimer's disease. Neurobiol. Aging 57, 8e17.

Smith SM, Jenkinson M, Johansen-Berg H, Rueckert D, Nichols TE, Mackay CE, Watkins KE, Ciccarelli O, Cader MZ, Matthews PM, Behrens TEJ, 2006 Tract-based spatial statistics: voxelwise analysis of multi- subject diffusion data. Neuroimage 31, 1487e1505.

Stricker NH, Salat DH, Kuhn TP, Foley JM, Price JS, Westlye LT, Esterman MS, McGlinchey RE, Milberg WP, Leritz EC, 2016 Mild cognitive impairment is associated with white matter integrity changes in late- myelinating regions within the corpus callosum. Am. J. Alzheimers Dis. Other Demen 31, 68e75.

Sullivan EV, Pfefferbaum A, 2006 Diffusion tensor imaging and aging. Neurosci. Biobehav. Rev 30, 749e761.

Tabesh A, Jensen JH, Ardekani BA, Helpern JA, 2011 Estimation of tensors and tensor-derived measures in diffusional kurtosis imaging. Magn. Reson. Med 65, 823e836.

Tsang A, Lebel CA, Bray SL, Goodyear BG, Hafeez M, Sotero RC, McCreary CR, Frayne R, 2017 White matter structural connectivity is not correlated to cortical Resting-state functional connectivity over the healthy adult lifespan. Front. Aging Neurosci 9, 144. [PubMed: 28572765]

Veraart J, Fieremans E, Jelescu IO, Knoll F, Novikov DS, 2016a Gibbs ringing in diffusion MRI: Gibbs ringing in diffusion MRI. Magn. Reson. Med 76, 301e314.

Veraart J, Novikov DS, Christiaens D, Ades-aron B, Sijbers J, Fieremans E, 2016b Denoising of diffusion MRI using random matrix theory. Neuroimage 142, 394e406.

Vidal-Piñeiro D, Walhovd KB, Storsve AB, Grydeland H, Rohani DA, Fjell AM, 2016 Accelerated longitudinal gray/white matter contrast decline in aging in lightly myelinated cortical regions: aging GWC Decline Relates to Myelin Con- tent. Hum. Brain Mapp 37, 3669e3684.

Weintraub S, Salmon D, Mercaldo N, Ferris S, Graff-Radford NR, Chui H, Cummings J, DeCarli C, Foster NL, Galasko D, Peskind E, Dietrich W, Beekly DL, Kukull WA, Morris JC, 2009 The Alzheimer's disease Centers' uniform data set (UDS): the neuropsychologic test battery. Alzheimer Dis. Assoc. Disord 23, 91e101.

Winkler AM, Ridgway GR, Webster MA, Smith SM, Nichols TE, 2014 Per- mutation inference for the general linear model. Neuroimage 92, 381e397.

Wolff JL, Starfield B, Anderson G, 2002 Prevalence, expenditures, and compli- cations of multiple chronic conditions in the elderly. Arch. Intern. Med 162, 2269e2276.

Xia M, Wang J, He Y, 2013 BrainNet viewer: a network visualization tool for human brain connectomics. PLoS One 8, e68910. [PubMed: 23861951]

Yeatman JD, Wandell BA, Mezer AA, 2014 Lifespan maturation and degenera- tion of human brain white matter. Nat. Commun 5, 4932. [PubMed: 25230200]

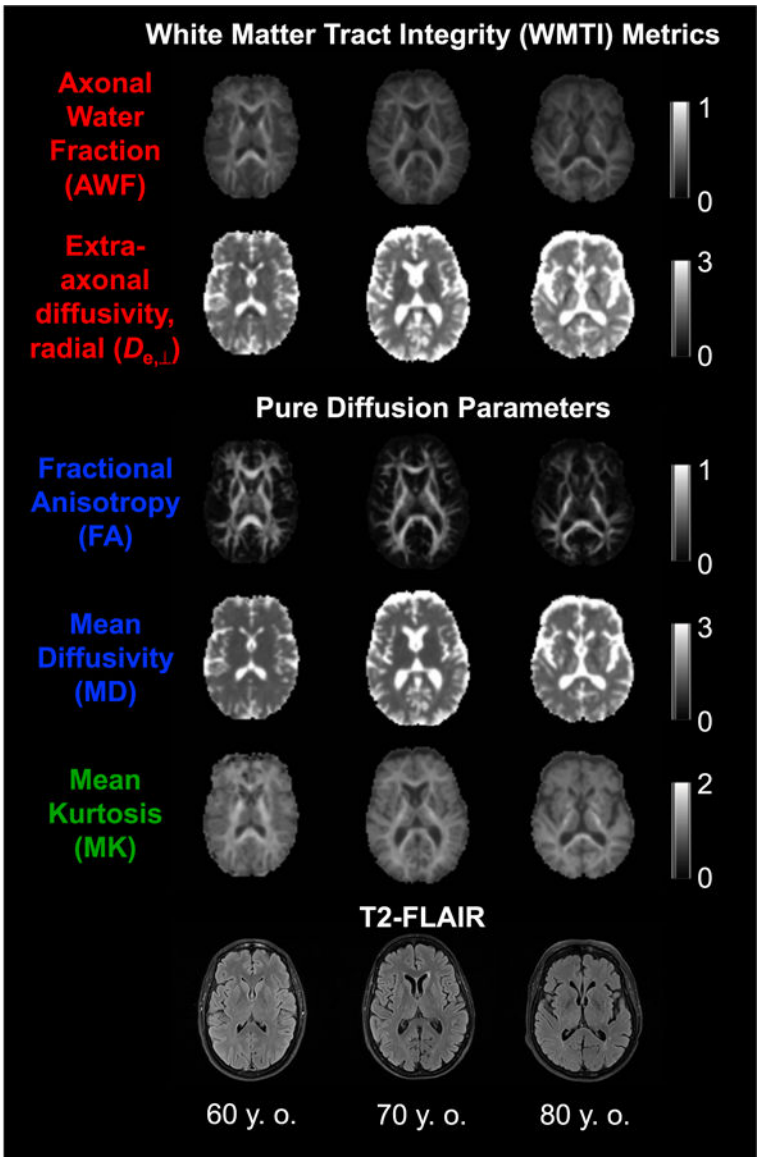

Fig. 1.

Metrics obtained using DKI. DKI parametric maps and T2-FLAIR images of 60-, 70-, and 80-year-old participants (all female, white, and right-handed). The calibration bars for the diffusivities are in units of mm2/ms, whereas those for the AWF, FA, and MK are dimensionless. Abbreviations: AWF, axonal water fraction; DKI, diffusional kurtosis imaging; FA, fractional anisotropy; MK, mean kurtosis.

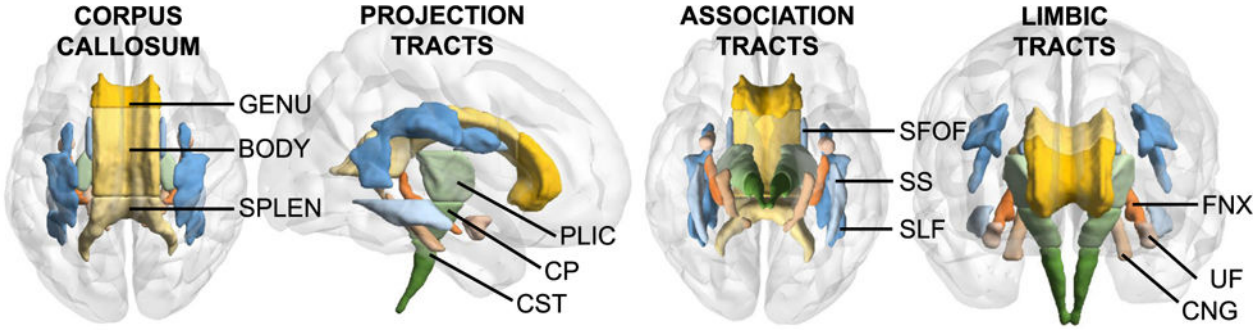

Fig. 2.

Regions of interest. From left to right: corpus callosum tracts, superior view; projection tracts, from right; association tracts, inferior view, and limbic tracts, anterior view. Abbreviations: BODY, body; CP, cerebral peduncles; CST, corticospinal tract; CNG, cingulum (hippocampus); FNX, fornix (cres); GENU, genu; PLIC, posterior limb of the internal capsule; SPLEN, splenium; SLF, superior longitudinal fasciculus; SS, sagittal stratum; SFOF, superior fronto-occipital fasciculus; UF, uncinate fasciculus.

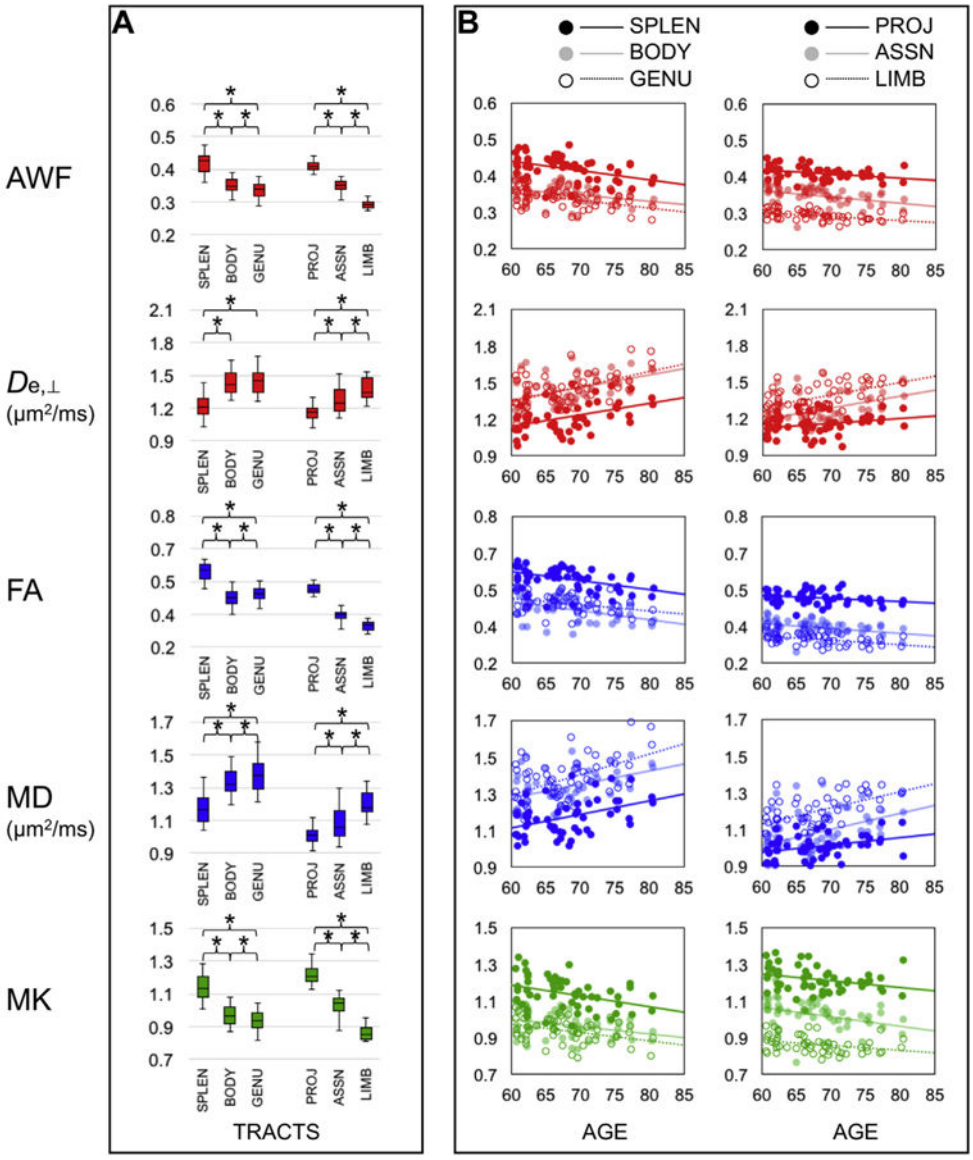

Fig. 3.

WMTI (red), DTI (blue), and DKI (green) metrics reflect ontogeny and age-related changes in white matter ($N = 54$). (A) Box plots (whiskers = 5th, 95th percentiles) of metric values in the corpus callosum and other tract ROI. (B) Scatterplots and linear regression lines illustrating the main findings per metric (y-axis) by age (x-axis). Abbreviations: ASSN, association tracts; AWF, axonal water fraction; BODY, body; $D_{e,\perp}$, extraaxonal diffusivity in the radial direction; DTI, diffusion tensor imaging; DKI, diffusional kurtosis imaging; FA, fractional anisotropy; GENU, genu; LIMB, limbic tracts; MD, mean diffusivity; MK, mean kurtosis; PROJ, projection tracts; ROI, region-of-interest; SPLEN, splenium; WMTI, white matter tract integrity. *$p < 0.01$. (For interpretation of the references to color in this figure legend, the reader is referred to the Web version of this article.)

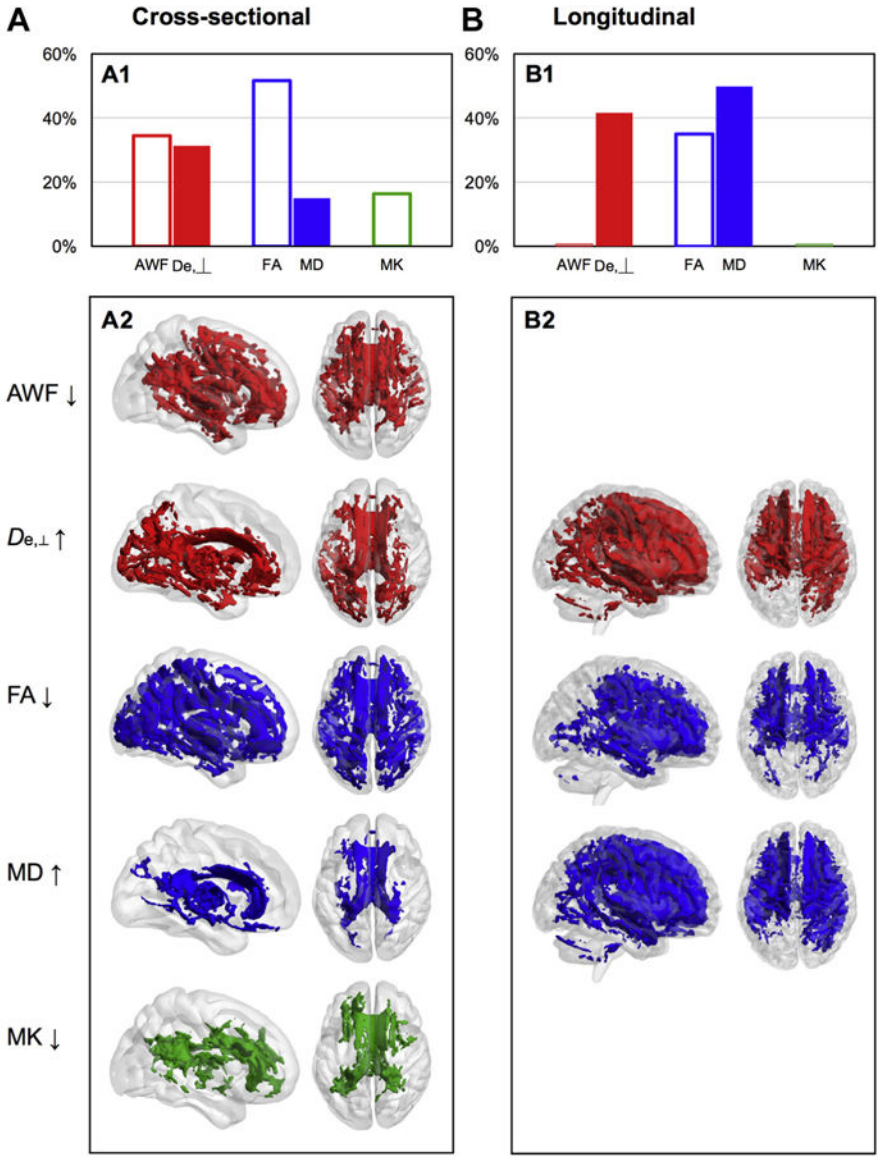

Fig. 4.

Voxelwise results of age-related changes in WMTI (red), DTI (blue), and DKI (green) metrics. Percentage of white matter skeleton voxels that (A1) significantly correlated with age and (B1) significantly changed with age over time, for each metric, where filled bars = positive correlations/increase and empty bars = negative correlations/decrease. TBSS results indicating voxels that (A2) significantly correlated with age and (B2) significantly changed, for each metric, where left brain = view from right and right brain = superior view. Abbreviations: AWF, axonal water fraction; $D_{e,\perp}$, extraaxonal diffusivity in the radial direction; DKI, diffusional kurtosis imaging; DTI, diffusion tensor imaging; FA, fractional anisotropy; MD, mean diffusivity; MK, mean kurtosis; WMTI, white matter tract integrity. (For interpretation of the references to color in this figure legend, the reader is referred to the Web version of this article.)

Table 1

Participant demographics and medical history

	Cross-sectional sample (*N* = 54) n (%)	**Longitudinal sample, baseline (*n* = 39) n (%)**	**Longitudinal sample, follow-up (*n* = 39) n (%)**
Age *	67.8 ± 5.5, 67.1 (60.6–80.4)	67.7 ± 5.1, 67.2 (60.7–80.3)	69.0 ± 5.2, 68.2 (61.8–81.9)
Female	34 (63.0)	28 (71.8)	-
Right-handed	49 (90.7)	37 (94.9)	-
White	49 (90.7)	35 (89.7)	-
Years of education *	16.4 ± 2.5, 17.0 (12–20)	16.5 ± 2.5, 18.0 (12–20)	-
MoCA *	27.0 ± 1.7, 27.0 (23–30)	27.0 ± 1.6, 27.0 (23–30)	26.7 ± 2.0, 27.0 (23–30)
BMI *	28.5 ± 6.4, 27.2 (18.9–49.5)	27.8 ± 6.2, 25.3 (18.9–47.6)	27.3 ± 5.8, 25.5 (19.0–45.8)
Depression	8 (14.8)	6 (15.4)	3 (7.7)
Diabetes	7 (13.0)	6 (15.4)	6 (15.4)
Dyslipidemia	16 (29.6)	11 (28.9)	13 (33.3)
Hearing Loss	16 (29.6)	10 (25.6)	10 (25.6)
Heart disease	3 (5.6)	2 (5.1)	7 (17.9)
Hypertension	22 (40.7)	17 (43.6)	16 (41.0)
Sleep disorder	13 (24.1)	9 (23.1)	9 (23.1)
Thyroid disease	8 (14.8)	5 (12.8)	5 (12.8)
Smoking (ever)	31 (57.4)	23 (59.0)	22 (56.4)
Estrogen use (ever)	24 (44.4)	19 (48.7)	20 (51.3)

Variables indicated by an * present the following values: mean ± SD, median (min-to-max).

Discrepancies between presumably static variables (i.e., Smoking [ever] and Estrogen use [ever]) between baseline and follow-up in the longitudinal sample are likely attributable to methodological limitations of collecting medical history through self-report.

Key: BMI, body mass index; MoCA, montreal cognitive assessment.

Table 2

Within-subjects general linear model results testing differences in baseline metrics among corpus callosum and other tracts ($N = 54$)

Metric	**Corpus callosum tracts**			***F* (df)**	***p*-value**	χ^2
	Splenium, Mean (SD)	**Body, Mean (SD)**	**Genu, Mean (SD)**			
AWF	0.42 (0.03)	0.35 (0.03)	0.34 (0.03)	858.88 (1.56[a])	<0.001	0.94
$D_{e,\perp}$	1.21 (0.12)	1.44 (0.12)	1.44 (0.13)	322.72 (1.71[a])	<0.001	0.86
FA	0.54 (0.05)	0.42 (0.05)	0.44 (0.04)	788.19 (1.79)	<0.001	0.94
MD	1.17 (0.10)	1.33 (0.09)	1.38 (0.12)	294.59 (1.63)	<0.001	0.85
MK	1.14 (0.09)	0.97 (0.07)	0.94 (0.07)	576.56 (2)	<0.001	0.96
Metric	Other tracts			*F* (df[a])	*p*-value	χ^2
	Projection, Mean (SD)	Association, Mean (SD)	Limbic, Mean (SD)			
AWF	0.41 (0.02)	0.35 (0.03)	0.29 (0.01)	1217.83 (1.51[a])	<0.001	0.96
$D_{e,\perp}$	1.15 (0.08)	1.27 (0.13)	1.37 (0.11)	257.04 (1.61[a])	<0.001	0.83
FA	0.47 (0.03)	0.35 (0.03)	0.30 (0.02)	2807.71 (2)	<0.001	0.99
MD	1.01 (0.06)	1.08 (0.11)	1.20 (0.08)	246.15 (1.62)	<0.001	0.82
MK	1.22 (0.06)	1.03 (0.08)	0.86 (0.05)	2060.21 (1.45)	<0.001	0.95

Means across all rows were significantly different from each other at $p < 0.01$ with Bonferroni adjustment for multiple comparisons, except for $D_{e,\perp}$ in the body and splenium (p = ns).

Key: AWF, axonal water fraction; FA, fractional anisotropy; MD, mean diffusivity; MK, mean kurtosis.

[a]Greenhouse-Geissereadjusted degrees of freedom for violating the assumption of sphericity.

Table 3

Linear mixed-effects model results using cross-sectional baseline data ($N = 54$)

	AWF, Estimate (CI)	$D_{e,\perp}$, Estimate (CI)	FA, Estimate (CI)	MD, Estimate (CI)	MK, Estimate (CI)
Corpus callosum tracts					
Intercept	0.48[a] (0.39–0.57)	0.72[a] (0.38–1.07)	0.67[a] (0.54–0.80)	0.62[a] (0.31–0.94)	1.27[a] (1.04–1.49)
Splenium	0.08[a] (0.08–0.09)	−0.23[a] (−0.25 to 0.21)	0.10[a] (0.09–0.10)	−0.04 (−0.18 to 0.26)	0.21[a] (0.19–0.22)
Body	0.01[b] (0.01–0.02)	−0.00 (−0.03 to 0.02)	−0.02 (−0.03 to 0.02)	−0.21 (−0.01 to 0.43)	0.03[a] (0.02–0.04)
Genu	0.00	0.00	0.00	0.00	0.00
Age	−0.00[a] (−0.00 to 0.00)	0.01[a] (0.01e0.01)	−0.00[b] (−0.01 to 0.00)	0.01[a] (0.01–0.02)	−0.01[b] (−0.01 to 0.00)
Splenium[c] age				−0.00c (−0.01 to 0.00)	
Body[c] age				−0.00c (−0.01 to 0.00)	
Other tracts					
Intercept	0.38[a] (0.33–0.44)	0.68[a] (0.35–1.00)	0.41[a] (0.33–0.49)	0.61[a] (0.35–0.87)	1.12[a] (0.95–1.29)
Projection	0.12[a] (0.11–0.12)	0.20 (−0.02 to 0.43)	0.17[a] (0.16–0.17)	0.13 (−0.07 to 0.34)	0.36[a] (0.34–0.37)
Association	0.06[a] (0.05–0.06)	−0.06 (−0.28 to 0.17)	0.05[a] (0.04–0.05)	−0.13 (−0.33 to 0.08)	0.16[a] (0.15–0.18)
Limbic	0.00	0.00	0.00	0.00	0.00
Age	−0.00[b] (−0.00 to 0.00)	0.01[a] (0.01–0.02)	−0.00[b] (−0.00 to 0.00)	0.01[a] (0.0–0.01)	−0.00[b] (−0.01 to 0.00)
Projection[c] age		−0.01[a] (−0.01 to 0.00)		−0.00[b] (−0.01 to 0.00)	
Association[c] age		−0.00 (−0.00 to 0.00)		−0.00 (−0.00 to 0.00)	

Key: AWF, axonal water fraction; CI, confidence intervals; FA, fractional anisotropy; MD, mean diffusivity; MK, mean kurtosis.

[a] $p < 0.001$.

[b] $p = 0.01$.

[c] $p < 0.05$.

Table 4

Within-subjects general linear model results testing differences in metrics expressed as annualized percent change from baseline among corpus callosum and other tracts (N=39)

Metric	**Corpus callosum tracts**			***F* (df)**	***p*-value**	χ^2
	Splenium, Mean % (SD)	**Body, Mean % (SD)**	**Genu, Mean % (SD)**			
AWF	−0.57 (1.99)	0.25 (3.05)	−0.37 (1.64)	2.59 (1.63[a])	0.08	0.06
$D_{e,\perp}$	0.10 (3.89)	0.46 (3.44)	0.99 (2.96)	1.44 (2)	0.25	0.07
FA	−0.74 (2.29)	−0.60 (3.78)	−1.17 (2.94)	1.28 (1.54[a])	0.28	0.03
MD	0.01 (3.19)	0.18 (3.26)	0.55 (3.02)	0.77 (1.71[a])	0.45	0.02
MK	−0.24 (2.94)	0.07 (2.63)	0.14 (1.98)	0.63 (1.72[a])	0.63	0.02
Metric	Other tracts			*F* (df)	*p*-value	χ^2
	Projection, Mean % (SD)	Association, Mean % (SD)	Limbic, Mean % (SD)			
AWF	−0.91 (2.48)	−0.39 (1.85)	−0.53 (3.17)	0.73 (1.71[a])	0.46	0.02
$D_{e,\perp}$	1.65 (4.50)	1.66 (2.73)	1.27 (3.37)	0.84 (2)	0.44	0.04
FA	−1.93 (2.66)	−1.04 (2.21)	−0.96 (2.35)	4.14 (1.57[a])	0.03	0.10
MD	1.36 (3.58)	1.47 (2.01)	1.07 (2.63)	0.62 (1.57[a])	0.50	0.02
MK	−0.25 (3.32)	0.12 (2.16)	0.02 (3.64)	0.30 (1.68[a])	0.70	0.01

Means across all rows were not significantly different from each other following Bonferroni adjustment for multiple comparisons, except for FA in projection and limbic tracts ($p < 0.05$).

Key: AWF, axonal water fraction; FA, fractional anisotropy; MD, mean diffusivity; MK, mean kurtosis.

[a]Greenhouse-Geissereadjusted degrees of freedom for violating the assumption of sphericity.